ACS APPLIED MATERIALS & INTERFACES

RESEARCH ARTICLE

www.acsami.org

TiO_2—B/Anatase Core—Shell Heterojunction Nanowires for Photocatalysis

Bin Liu, Ankur Khare, and Eray S. Aydil*

Department of Chemical Engineering and Materials Science, University of Minnesota, 421 Washington Avenue SE, Minneapolis, Minnesota 55455, United States

ABSTRACT: Fast separation and spatial control of electrons and holes after photogeneration is important in photocatalysis. Ideally, after photogeneration, electrons and holes must be segregated to different parts of the photocatalyst to take part in separate oxidation and reduction reactions. One way to achieve this is by building junctions into the catalyst with built-in chemical potential differences that tend to separate the electron and the hole into two different regions of the catalyst. In this work, we sought to accomplish this by controllably forming junctions between different phases of TiO_2. A synthesis method has been developed to prepare TiO_2—B core and anatase shell core—shell nanowires. We control the anatase phase surface coverage on the TiO_2—B core and show that the maximum photocatalytic activity is obtained when the solution containing the reactants can contact both the anatase and TiO_2—B phases. The photocatalytic activity drops both with bare TiO_2—B nanowires and with completely anatase covered TiO_2—B nanowires. In contrast, nanowires partially covered with anatase phase gives the highest photocatalytic activity. The improved photocatalytic activity is attributed to the effective electron—hole separation at the junction between the anatase and TiO_2—B phases.

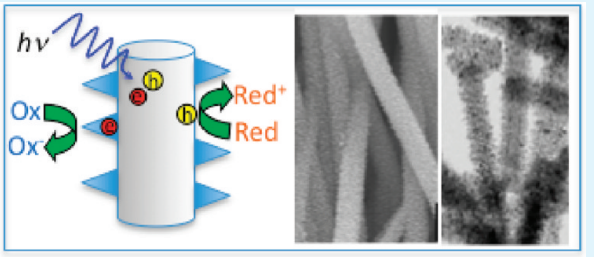

KEYWORDS: anatase, core—shell nanowires, photocatalysis, photocatalytic heterostructure, titanium dioxide, TiO_2(B) phase

INTRODUCTION

Since the discovery of photocatalytic water splitting reaction by Fujishima and Honda nearly 40 years ago,[1] titanium dioxide (TiO_2) has become the most widely studied photocatalyst.[2−6] Among the four polymorphs of TiO_2 found in nature, the anatase phase is the most photoactive because photogenerated charge carriers recombine at the lowest rate in anatase and many organic molecules readily interact with the anatase surfaces.[7−9] However, even in anatase, the recombination of photogenerated electrons and holes is still too fast, which results in low quantum efficiencies and limits the photocatalytic potential of anatase. An increase in electron and hole lifetime is expected to lead to higher quantum efficiency for steady-state photocatalysis.

To increase the photocatalytic reaction rates, the photogenerated electrons and holes must be separated into different locations on the catalyst. This can be achieved by building junctions and chemical potential gradients into the catalyst that tend to separate the electrons and the holes into two different regions of the catalyst.[10−27] Toward this end, TiO_2 based photocatalytic heterostructures such as anatase/rutile,[10−12] noble metal/TiO_2,[13−16] carbon/TiO_2,[17−19] metal oxide/TiO_2,[20−22] and metal chalcogenide/TiO_2[23−25] have been proposed and studied. After charge separation, photocatalytic oxidation and reduction reactions take place on different parts of the catalyst and both regions must be accessible to the reactants. Thus, in heterojunction photocatalysts where one component is grown or deposited on the other, one must have control over the coverage because both complete and sparse coverage of one component on the other will reduce the catalytic efficiency.

TiO_2—B is a metastable monoclinic phase of TiO_2 with an energy bandgap close to that of the anatase.[28−30] According to a recent theoretical calculation, the TiO_2—B valence band edge (VBE) is in the energy gap of the anatase phase, while its conduction band edge (CBE) is above the anatase CBE.[31] Thus, TiO_2—B and anatase form a type II heterojunction, and the electronic energy level differences can promote charge transfer from one phase to the other. During illumination, the CB of the anatase phase would attract the photogenerated electrons while the holes would seek the VB of the TiO_2—B phase.

In this Article, we describe a facile solution synthesis method to make TiO_2—B/anatase core—shell heterojunction nanowires. In this core—shell nanowire structure, anatase nanocrystals protrude along the anatase [001] crystallographic orientation from the surface of TiO_2—B nanowires. The coverage of the anatase nanocrystals on the TiO_2—B nanowire surfaces could be controlled easily by varying the synthesis time during the step when these nanocrystals are grown. Under UV illumination, the binary TiO_2 composite nanowires catalyze photodegradation of organic compounds by a factor of 5 faster than the control single component photocatalysts.

Received: August 19, 2011
Accepted: October 18, 2011
Published: October 18, 2011

EXPERIMENTAL SECTION

Materials Preparation. The nanowires with TiO_2−B core and anatase shell were grown on titanium foil via a four-step synthesis method. The first and second steps follow the method in our recent article.[32] Briefly, a piece of 0.127 mm thick titanium foil (1 cm × 2 cm) was cleaned ultrasonically for 30 min in a mixture of deionized water, acetone, and isopropanol (1:1:1 by volume) and placed at an angle against the wall of a 125 mL Teflon-lined stainless-steel autoclave (Parr Instrument Company) filled with 60 mL of 1 M aqueous NaOH solution. The autoclave was kept inside an electric oven at 220 °C for 48 h. This step grows a forest of 20 μm long sodium titanate ($Na_2Ti_2O_5 \cdot H_2O$) nanowires on the titanium foil.[32] Following, the autoclave was cooled, and the titanium foil covered with sodium titanate nanowires was taken out of the autoclave and immersed in 50 mL of 0.6 M HCl solution for 30 min to exchange Na^+ with H^+. This transforms the sodium titanate nanowires to hydrogen titanate ($H_2Ti_2O_5 \cdot H_2O$) nanowires. The hydrogen titanate nanowire covered foil was washed thoroughly with a copious amount of deionized water. In the third step, the hydrogen titanate nanowire covered titanium foil was placed into 100 mL of $TiCl_4$ solution and maintained at 50 °C for 0.5 to 24 h to grow anatase nanocrystals around the periphery of the nanowires. The duration of this growth step determined the coverage of anatase nanocrystals on the TiO_2−B nanowires. The $TiCl_4$ solution was prepared by mixing 0.09 mL of $TiCl_4$ with 0.4 mL of concentrated HCl solution (36.5−38% by weight) followed by adding deionized water to reach a final volume of 100 mL. Finally, the $H_2Ti_2O_5 \cdot H_2O$ nanowires on titanium foil partially or completely covered with anatase nanocrystals were calcined in a furnace at 500 °C for 2 h to convert the $H_2Ti_2O_5 \cdot H_2O$ phase to the TiO_2−B phase. This annealing did not change the phase of the anatase nanocrystals on the nanowires. For comparison, phase-pure anatase photocatalyst was prepared by calcining the $H_2Ti_2O_5 \cdot H_2O$ nanowires or $H_2Ti_2O_5 \cdot H_2O$/anatase core−shell nanowires on titanium foil at 650 °C for 2 h. In addition, phase-pure TiO_2−B nanowires were prepared by calcining the $H_2Ti_2O_5 \cdot H_2O$ nanowires on titanium foil at 500 °C for 2 h.[33] Nanowires were ultrasonically detached from the titanium foil for use in photodegradation reactions.

Photodegradation Reactions. In a typical experiment, 20 mg of nanowires ultrasonically detached from the titanium foil were added to 45 mL of deionized water in a 100 mL beaker. The mixture was ultrasonicated for 30 min over a water bath to disperse the catalyst nanowires. Following, 5 mL of 100 mg/L methyl orange solution, which had been bubbled with air for 1 h prior to use, was added to the nanowire dispersion. The photocatalyst methyl orange mixture was then stirred in the dark at room temperature for 30 min and later illuminated with a UV lamp (Mineralight Lamp, Model UVGL-25) for 60 min. Methyl orange can adsorb on the nanowires, which may result in a decrease in the solution concentration and the optical density of the solution. To eliminate this background effect, we carried out the photodegradation reaction after mixing the nanowires with the methyl orange solution in the dark for half an hour to reach the adsorption equilibrium. During the illumination, 2 mL of solution together with the catalyst was drawn out every 10 min to determine the concentration of the remaining methyl orange using UV−visible spectroscopy; the solution was separated from the catalyst through syringe filtration. The photodegradation reaction was carried out at neutral pH and nominally at room temperature without intentional heating or cooling.

Materials Characterization. The crystal structure of the nanowires from each synthesis step was investigated by X-ray diffraction (XRD) in a Bruker-AXS Microdiffractometer (Model D5005) with Cu Kα radiation (λ = 1.5406 Å) from 5° to 80° at a scanning speed of 2.4° min^{-1}. X-ray tube voltage and current were set at 45 kV and 40 mA, respectively.[34] The morphology and chemical composition of the nanowires were examined using field emission scanning electron microscopy (FESEM, JSM-6700F), transmission electron microscopy (TEM, FEI Tecnai T12, 120 kV), selected area electron diffraction (SAED), high-resolution transmission electron microscopy, and energy dispersive X-ray spectroscopy (HRTEM/EDX, FEI Tecnai G2 30, 300 kV). The nitrogen adsorption/desorption isotherms of the nanowires were measured on a Micrometrics ASAP 2000 system at 77 K. Prior to measurements, the nanowires were degassed at 353 K overnight. The concentration of methyl orange during photodegradation reaction was monitored with a UV−vis−NIR scanning spectrophotometer. The spectrophotometer included a combination of deuterium and tungsten halogen lamps (Ocean Optics, DH-2000-Ball) and a spectrometer (Ocean Optics, HR 2000), sensitive in the 200−1100 nm range, equipped with a grating and a silicon detector.[35]

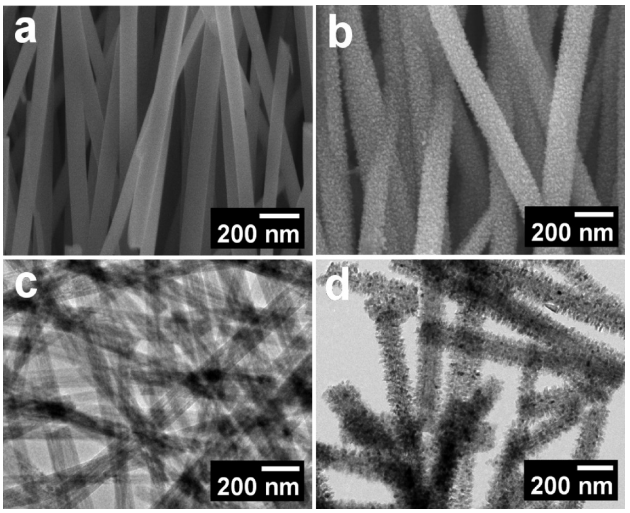

Figure 1. (a and c) FESEM and TEM images of the hydrogen titanate ($H_2Ti_2O_5 \cdot H_2O$) nanowires which were grown hydrothermally at 220 °C for 48 h. (b and d) FESEM and TEM images of TiO_2−B/anatase core−shell nanowires prepared by growing anatase nanocrystals on hydrogen titanate nanowires through immersion in $TiCl_4$ solution for 24 h at 50 °C and by calcining the product at 500 °C for 2 h.

RESULTS AND DISCUSSION

Hydrogen titanate ($H_2Ti_2O_5 \cdot H_2O$) nanowires grown on titanium foil through a two-step hydrothermal method form the backbone of the photocatalyst. The detailed morphological and structural characteristics of these nanowires were reported recently.[32] The $H_2Ti_2O_5 \cdot H_2O$ nanowires are single crystalline, and their axes are oriented along the [010] crystallographic direction. Following Yang and Zeng, we grow anatase nanocrystals on the periphery of these nanowires to form core−shell $H_2Ti_2O_5 \cdot H_2O$/anatase nanocomposites.[36] After the anatase growth step, the $H_2Ti_2O_5 \cdot H_2O$ nanowire cores were converted to TiO_2−B phase by calcination at 500 °C. During this step, the anatase nanocrystals on the periphery of the TiO_2−B nanowires remain unchanged. Figure 1 shows FESEM and TEM images of typical TiO_2−B/anatase core−shell nanowires prepared by immersing hydrogen titanate nanowires in $TiCl_4$ solution for 24 h to grow anatase nanocrystals, followed by calcination at 500 °C for 2 h. The TiO_2−B nanowires are covered with closely packed rod-like anatase crystallites. The average diameter of the core−shell nanowires is approximately 150 nm, larger than the initial hydrogen titanate nanowire diameter (~100 nm). The contrast between the core and the shell is clearly visible in the TEM image displayed in Figure 1d.

Figure 2 shows the XRD from nanowires after each synthesis step. The diffraction pattern in Figure 2b agrees well with the body-centered orthorhombic (BCO) $H_2Ti_2O_5 \cdot H_2O$ phase, which consists of two-dimensional sheets of edge sharing TiO_6 octahedra.[32] After the anatase nanocrystal growth, despite the proximity of diffraction peaks from $H_2Ti_2O_5 \cdot H_2O$ and anatase, one can clearly detect well-resolved anatase diffractions,

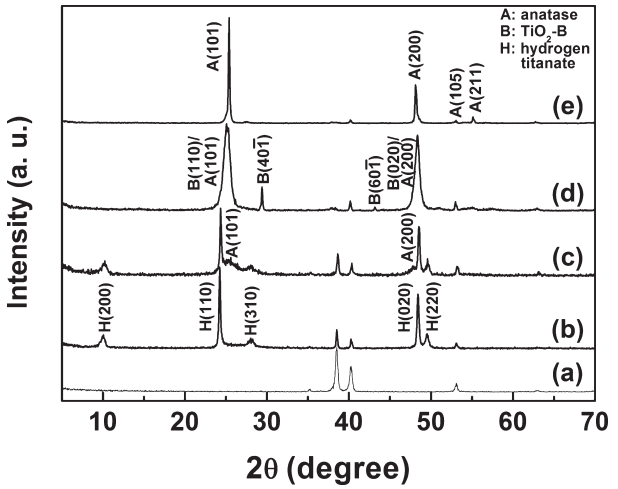

Figure 2. XRD patterns from (a) titanium foil, (b) the $H_2Ti_2O_5 \cdot H_2O$ nanowires, (c) $H_2Ti_2O_5 \cdot H_2O$/anatase core−shell nanowires, (d) TiO_2−B/anatase core−shell nanowires, and (e) anatase nanowires.

consistent with the presence of anatase nanocrystals on the hydrogen titanate nanowires. The (110) and (020) diffractions from $H_2Ti_2O_5 \cdot H_2O$ overlap with the (101) and (200) diffractions from anatase, respectively. The broad width of the anatase diffraction peaks indicates that the anatase crystallites have sizes on the order of nanometers. During calcination at 500 °C, the $H_2Ti_2O_5 \cdot H_2O$ nanowire core is converted to TiO_2−B while anatase nanocrystal shell remains unchanged. Figure 2d shows diffraction peaks from both anatase and TiO_2−B. If the calcination temperature is raised to 650 °C, the $H_2Ti_2O_5 \cdot H_2O$ nanowires are transformed to anatase nanowires and the entire structure becomes anatase. In this case, only the anatase diffractions are observed as shown in Figure 2e.

The crystal structure of the TiO_2−B/anatase core−shell nanowires was also examined using selected area electron diffraction (SAED) and high-resolution transmission electron microscopy (HRTEM). Figure 3a,b shows a TEM image of a TiO_2−B/anatase core−shell nanowire and its corresponding SAED pattern, respectively. A careful examination of the SAED shows that it is a superimposition of two sets of diffraction patterns. The first set of diffraction spots originates from the TiO_2−B nanowire core and indicates that the TiO_2−B nanowire is single crystal and is oriented in the [010] direction. The second set of diffraction spots originates from the anatase nanocrystal shell. The orientation of this second spot pattern with respect to that from the TiO_2−B phase suggests that the anatase nanocrystals on the TiO_2−B nanowire grow along the anatase *c*-axis; this conclusion is confirmed using HRTEM. For example, Figure 3c shows an HRTEM image captured near the interface

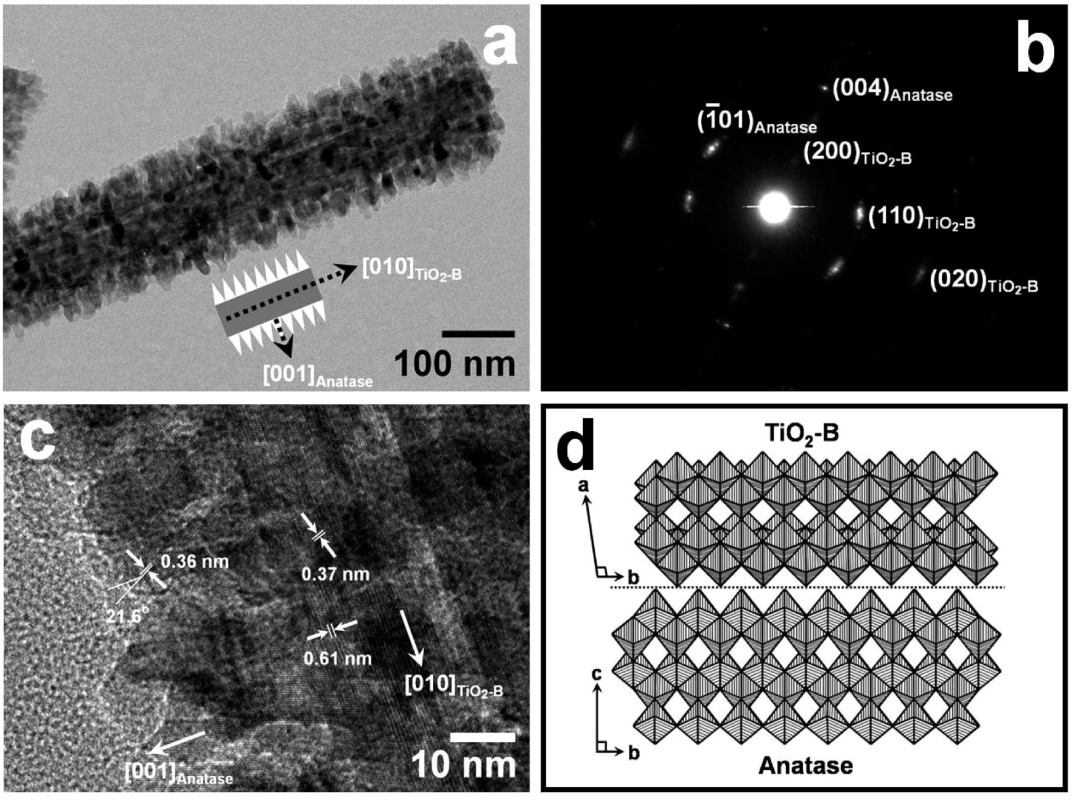

Figure 3. (a, b, and c) TEM image of a TiO_2−B/anatase core−shell nanowire, its corresponding SAED pattern and HRTEM image, respectively. (d) The schematic representation of the interface between TiO_2−B and anatase. The octahedra represent the TiO_6 octahedra. Inset in part (a) indicates the relative orientations of anatase nanocrystals (white) and the TiO_2−B nanowire core.

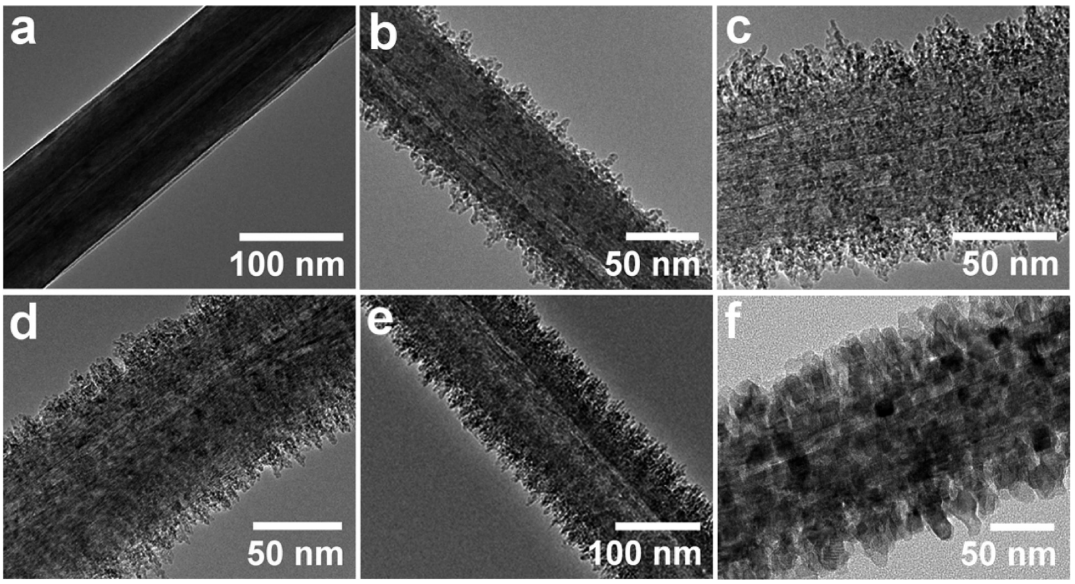

Figure 4. TEM images of TiO_2−B/anatase core−shell nanowires prepared by treating $H_2Ti_2O_5 \cdot H_2O$ nanowires in $TiCl_4$ solution for different times, followed by calcination at 500 °C for 2 h: (a) 0 h, (b) 1 h, (c) 1.5 h, (d) 2 h, (e) 8 h, and (f) 24 h.

between the anatase nanocrystals and the TiO_2−B nanowire. The interplanar spacing from both TiO_2−B nanowire core with $d_{(200)}$ = 0.61 nm and $d_{(110)}$ = 0.37 nm and anatase nanocrystal shell with $d_{(101)}$ = 0.36 nm are clearly visible. Furthermore, the measured angle between the anatase ⟨101⟩ and ⟨001⟩ is approximately 21.6° and matches nearly exactly to the theoretical value of 21.7°. Thus, the HRTEM measurement confirms that the TiO_2 nanocrystals on the TiO_2−B nanowire are single-crystalline anatase and grow along the [001] direction. The lattice mismatch between the TiO_2−B (b = 3.7412 Å)[37] and anatase ($a = b$ = 3.7852 Å)[17] is ∼1%. We believe that this small lattice mismatch promotes the epitaxial nucleation and growth of anatase TiO_2 nanocrystals on the TiO_2−B nanowires. The (001) plane of anatase nanocrystal connects the (100) plane of TiO_2−B nanowire to form a coherent interface. The schematic illustration of the interface derived on the basis of the HRTEM observations is displayed in Figure 3d, which shows that the anatase and TiO_2−B crystal structures are well-matched at the atomic level when the (001) plane of the anatase nanocrystal and (100) plane of the TiO_2−B nanowire are parallel; such a smooth transition from one crystal phase to the other could minimize the formation of interfacial defects, which should benefit the interfacial charge transfer after photogeneration.

The size and coverage of the anatase nanocrystals on the surface of the TiO_2−B nanowires could be varied by changing the anatase growth time. Figure 4 shows the TEM images of the TiO_2−B/anatase core−shell nanowires for different growth durations in the $TiCl_4$ solution. When the growth duration in $TiCl_4$ solution is short (e.g., 1 h), the anatase nanocrystals growing on the TiO_2−B nanowires are well separated. The anatase nanocrystals are ∼15 nm long in the direction perpendicular to the TiO_2−B nanowire axis and approximately 5 nm in diameter. The interface between the TiO_2−B and the anatase phases is clearly visible in Figure 4b. As the growth duration in $TiCl_4$ solution increases, the coverage of the anatase nanocrystals on the TiO_2−B nanowire's periphery increases dramatically. At the same time, the anatase nanocrystals grow larger. For example, after 24 h of growth in $TiCl_4$ solution, the diameter and the length of the anatase nanocrystals increase from ∼5 nm to ∼15 nm and from ∼15 nm to ∼30 nm, respectively. The anatase shell densifies as nanocrystal size and coverage increase, and TiO_2−B/anatase interface becomes less apparent.

The degradation of methyl orange was chosen as a model reaction to investigate the photocatalytic activity of the TiO_2−B/anatase core−shell nanowire catalyst. The photocatalytic methyl orange is thought to degrade via the following reactions:

$$TiO_2\text{−B/anatase} + h\nu \rightarrow TiO_2\text{−B/anatase}(e^- + h^+)$$

$$h^+ + OH^- \rightarrow OH\cdot$$

$$e^- + O_2 \rightarrow O_2^-$$

$$O_2^- + H_2O \rightarrow HO_2\cdot + OH^-$$

$$HO_2\cdot + H_2O \rightarrow H_2O_2 + OH\cdot$$

$$H_2O_2 \rightarrow 2OH\cdot$$

$$OH\cdot + \text{methylorange} \rightarrow \text{products}$$

This reaction is chosen because both the electron and hole end up participating in the production of OH radical, which degrades the methyl orange. Moreover, the extent of the reaction can be monitored through optical absorption. Figure 5a shows the decay of methyl orange concentration as a function of illumination time in an aqueous solution with and without photocatalyst particles. It is clear that the TiO_2−B/anatase core−shell nanowire catalyst has the highest photocatalytic activity: solution that contained the TiO_2−B/anatase core−shell nanowires showed the fastest methyl orange concentration decay. Photodegradation reaction can be described using a pseudofirst-order reaction kinetics,[38,39] and the temporal evolution of the methyl orange concentration as a function of time, $C(t)$, is given by

$$\ln(C(t)/C_o) = -kt$$

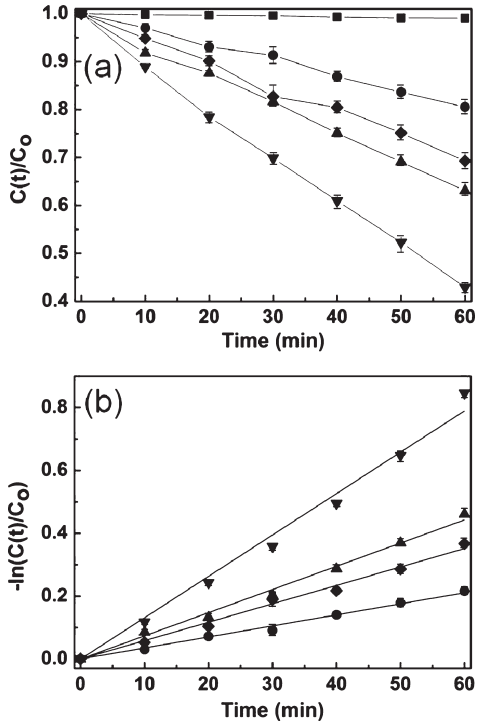

Figure 5. Photocatalytic degradation of methyl orange with different TiO_2 photocatalyst under UV illumination: (a) normalized concentration ($C(t)/C_o$) versus time; (▼): TiO_2−B/anatase core−shell nanowires prepared by growing anatase shell for 1 h in $TiCl_4$ solution; (▲): anatase/anatase core−shell nanowires prepared by calcining the $H_2Ti_2O_5 \cdot H_2O$/anatase core−shell nanowires at 650 °C for 2 h; (◆): anatase nanowires prepared by calcining $H_2Ti_2O_5 \cdot H_2O$ nanowires at 650 °C for 2 h; (●): TiO_2−B nanowires prepared by calcining $H_2Ti_2O_5 \cdot H_2O$ nanowires at 500 °C for 2 h; and (■): control experiment with no catalyst. (b) Semilog plots based on the data in (a) to obtain the first-order photodegradation reaction rate coefficient.

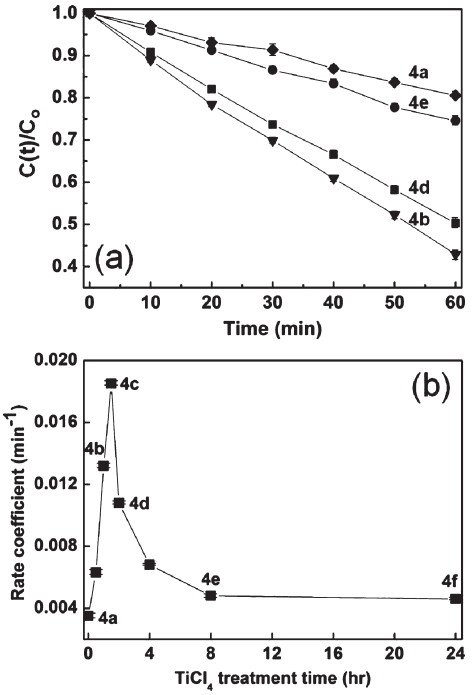

Figure 6. Photocatalytic degradation of methyl orange with TiO_2−B/anatase core−shell nanowire photocatalyst prepared by growing anatase shell for different durations in $TiCl_4$ solution. Coverage of anatase nanocrystals on TiO_2−B nanowire core increases monotonically with increasing $TiCl_4$ treatment time. (a) Normalized concentration ($C(t)/C_o$) versus degradation time. (b) Photodegradation rate coefficient versus anatase growth time and, hence, anatase nanocrystal coverage in $TiCl_4$ solution. Labels refer to TEM images shown in Figure 4.

where C_o is the initial concentration of methyl orange solution and k is the photocatalytic degradation rate coefficient. Photocatalytic activity is quantified using the photodegradation rate coefficient which was determined from the slopes of $-\ln(C(t)/C_o)$ vs t as shown in Figure 5b. The rate coefficient for the TiO_2−B/anatase core−shell nanowire photocatalyst is more than double the rate coefficient for the control photocatalyst, which included bare TiO_2−B nanowires, bare anatase nanowires, and anatase/anatase core−shell nanowires. The anatase/anatase core−shell nanowires were prepared by calcining $H_2Ti_2O_5 \cdot H_2O$/anatase core−shell nanowires at 650 °C for 2 h. The specific surface area of TiO_2−B/anatase core−shell nanowires (19.8 g/m^2) was approximately the same as that of the anatase/anatase core−shell nanowires (19.4 g/m^2). Moreover, the anatase nanocrystals on the surface of the nanowires have the same crystal orientation in both cases. The surface areas of TiO_2-B/anatase core−shell nanowires increased slowly and monotonically with reaction time in $TiCl_4$ solution. For example, the specific surface areas of TiO_2−B/anatase core−shell nanowires shown in Figure 4a,b,d,e were 14.1 m^2/g (no growth), 19.8 m^2/g, 22.2 m^2/g, and 26.9 m^2/g (8 h growth), respectively. For comparison, the specific surface area of the anatase/anatase core−shell nanowires was 19.4 m^2/g. An increase in catalyst surface area will increase the photocatalytic activity. However, the specific surface area increase can be neither the main nor the sole reason for explaining the experimental results in Figures 5 and 6. First, head-to-head comparison of TiO_2-B/anatase core−shell nanowires with anatase/anatase core−shell nanowires with the same specific surface area (19.8 m^2/g and 19.4 m^2/g, respectively) shows that the rate constant is more than doubled for TiO_2-B/anatase core−shell nanowires (Figure 5). Second, as shown in Figure 6b, the photocatalytic activity reaches the maximum for catalyst nanowires with an intermediate surface area. Thus, the improvement in photocatalytic activity of the TiO_2−B/anatase core−shell nanowire photocatalyst should be attributed to factors other than an increase in specific surface area or change in the crystal orientation. We attribute the higher photocatalytic activity of the TiO_2−B/anatase core−shell nanowire photocatalyst to fast charge separation due to the energetic differences between TiO_2−B and anatase phases that increase the lifetimes of photogenerated charge carriers. In the anatase/anatase core shell nanowire photocatalyst, there is no driving force for charge separation and photogenerated charge carriers can recombine much faster without participating in reduction or oxidation reactions.

Growing the anatase shell for a long time in $TiCl_4$ solution (>4 h) completely covers the TiO_2−B nanowire core with anatase nanocrystals. Moreover, this anatase nanocrystal layer grows thicker with growth duration. This thick and dense coating of anatase nanocrystals reduces the reactant access to the photogenerated holes in the TiO_2−B nanowire core. Since both oxidation and reduction reactions have to occur to prevent charge buildup on the catalyst surface, the photocatalytic activity of the TiO_2−B/anatase core−shell nanowires where the anatase

nanocrystals completely cover the TiO_2−B core would be limited by the hole consumption rate on the TiO_2−B surface. The anatase nanocrystal coverage on the TiO_2−B nanowire core was varied by changing the anatase nanocrystal growth time in the $TiCl_4$ solution. Figure 6a,b shows the changes in the photocatalytic activity of the TiO_2−B/anatase core−shell nanowires as a function of anatase nanocrystal growth time and, hence, as a function of nanocrystal coverage on the nanowire. The photocatalytic activity of the TiO_2−B/anatase core−shell nanowire photocatalyst first increases with increasing anatase nanocrystal coverage, reaches a maximum, and eventually decreases. We attribute this change in photocatalytic activity with respect to the anatase nanocrystal coverage to the trade-off between improved charge carrier lifetimes due to the formation of type II heterojunction and loss in the accessibility to the active sites on the TiO_2−B surface because of the densification of the external anatase shell. When the nanocrystal coverage is zero (bare TiO_2−B nanowire), there is no mechanism to separate the electron−hole pairs in the nanowire and some fraction of them recombine before participating in oxidation and reduction reactions. As the anatase nanocrystal coverage increases, photogenerated electron−hole pairs in the TiO_2−B phase can be separated by transferring the electron to the anatase nanocrystals. The holes remain in the TiO_2−B nanowire backbone. This increases the lifetimes of carriers and, consequently, photocatalytic efficiency. Since both electrons and holes participate in the degradation reactions, both TiO_2−B nanowire backbone and anatase nanocrystals must have access to the solution. As the anatase nanocrystal coverage increases, this access to the TiO_2−B nanowire is reduced and eventually blocked. The balance between these two competing effects produces the maximum in the photodegradation reaction coefficient as shown in Figure 6b.

CONCLUSIONS

In summary, we have developed a facile synthesis method to make TiO_2−B/anatase core−shell nanowire photocatalysts. The anatase nanocrystals protrude from the periphery of the TiO_2−B nanowire core along the anatase [001] crystallographic orientation. The TiO_2−B core and anatase shell form a type II heterojunction that facilitates efficient photogenerated charge carrier separation into different parts of the catalyst. Charge separation can reduce charge recombination and increase charge-carrier lifetime and, thus, enhance photocatalytic efficiency.

AUTHOR INFORMATION

Corresponding Author
*E-mail: aydil@umn.edu.

ACKNOWLEDGMENT

This work was supported partially by the Minnesota Initiative for Renewable Energy and the Environment (IREE) grant no. RS-0021-09. This work was supported partially by the MRSEC program of the National Science Foundation under award number DMR-0819885 and utilized the College of Science and Engineering characterization facility at the University of Minnesota, a member of the NSF-funded materials research facilities network.

REFERENCES

(1) Fujishima, A.; Honda, K. *Nature* **1972**, *106*, 4428.
(2) Fujishima, A.; Hashimoto, K.; Watanabe, H. *TiO_2 Photocatalysis: Fundamentals and Applications*; BKC, Inc.: Tokyo, 1999.
(3) Hoffmann, M. R.; Martin, S. T.; Choi, W. Y.; Bahnemann, D. W. *Chem. Rev.* **1995**, *95*, 69.
(4) Thompson, T. L.; Yates, J. T. *Chem. Rev.* **2006**, *106*, 4428.
(5) Chen, X.; Mao, S. S. *Chem. Rev.* **2007**, *107*, 2891.
(6) Carp, O.; Huisman, C. L.; Reller, A. *Prog. Solid State Chem.* **2004**, *32*, 33.
(7) Anpo, M.; Shima, T.; Kodama, S.; Kubokawa, Y. *J. Phys. Chem.* **1987**, *91*, 4305.
(8) Tanaka, K.; Capule, M. F. V.; Hisanage, T. *Chem. Phys. Lett.* **1991**, *187*, 73.
(9) Sclafani, A.; Herrmann, J. M. *J. Phys. Chem.* **1996**, *100*, 13655.
(10) Liu, Z. Y.; Zhang, X. T.; Nishimoto, S.; Jin, M.; Tryk, D. A.; Murakami, T.; Fujishima, A. *Langmuir* **2007**, *23*, 10916.
(11) Li, G. H.; Ciston, S.; Saponijic, Z. V.; Chen, L.; Dimitrijevic, N. M.; Rajh, T.; Gray, K. A. *J. Catal.* **2008**, *253*, 105.
(12) Zhang, J.; Xu, Q.; Feng, Z.; Li, M.; Li, C. *Angew. Chem., Int. Ed.* **2008**, *47*, 1766.
(13) (a) Li, J.; Zeng, H. C. *Angew. Chem., Int. Ed.* **2005**, *44*, 4342. (b) Li, J.; Zeng, H. C. *Chem. Mater.* **2006**, *18*, 4270.
(14) Tada, H.; Soejima, T.; Ito, S.; Kobayashi, H. *J. Am. Chem. Soc.* **2004**, *126*, 15952.
(15) (a) Yan, W. F.; Mahurin, S. M.; Pan, Z. W.; Overbury, S. H.; Dai, S. *J. Am. Chem. Soc.* **2005**, *127*, 10480. (b) Tian, Y.; Tatsuma, T. *J. Am. Chem. Soc.* **2005**, *127*, 7632.
(16) Awazu, K.; Fujimaki, M.; Rockstuhl, C.; Tominaga, J.; Murakami, H.; Ohki, Y.; Yoshida, N.; Watanabe, T. *J. Am. Chem. Soc.* **2008**, *130*, 1676.
(17) Liu, B.; Zeng, H. C. *Chem. Mater.* **2008**, *20*, 2711.
(18) Yao, Y.; Li, G.; Ciston, S.; Lueptow, R. M.; Gray, K. A. *Environ. Sci. Technol.* **2008**, *42*, 4952.
(19) Williams, G.; Seger, B.; Kamat, P. V. *ACS Nano* **2008**, *2*, 1487.
(20) Hou, Y.; Li, X. Y.; Zou, X. J.; Quan, X.; Chen, G. C. *Environ. Sci. Technol.* **2009**, *43*, 858.
(21) Yang, H. Y.; Yu, S. F.; Lau, S. P.; Zhang, X. W.; Sun, D. D.; Jun, G. *Small* **2009**, *5*, 2260.
(22) Tada, H.; Hattori, A.; Tokihisa, Y.; Imai, K.; Tohge, N.; Ito, S. *J. Phys. Chem. B* **2000**, *104*, 4585.
(23) Banerjee, S.; Mohapatra, S. K.; Das, P. P.; Misra, M. *Chem. Mater.* **2008**, *20*, 6784.
(24) Ratanatawanate, C.; Xiong, C. R.; Balkus, K. J., Jr. *ACS Nano* **2008**, *2*, 1682.
(25) Acharya, K. P.; Alabi, T. R.; Schmall, N.; Hewa-Kasakarage, N. N.; Kirsanova, M.; Nemchinov, A.; Khon, E.; Zamkov, M. *J. Phys. Chem. C* **2009**, *113*, 19531.
(26) Yang, D. J.; Liu, H. W.; Zheng, Z. F.; Yuan, Y.; Zhao, J. -C.; Waclawik, E. R.; Ke, X. B.; Zhu, H. Y. *J. Am. Chem. Soc.* **2009**, *131*, 17885.
(27) Wang, C. H.; Shao, C. L.; Zhang, X. T.; Liu, Y. C. *Inorg. Chem.* **2009**, *48*, 7261.
(28) Yin, S.; Wu, J. H.; Aki, M.; Sato, T. *Int. J. Inorg. Mater.* **2000**, *2*, 325.
(29) Kuo, H.-L.; Kuo, C.-Y.; Liu, C.-H.; Chao, J.-H.; Lin, C.-H. *Catal. Lett.* **2007**, *113*, 7.
(30) Kavan, L.; Grätzel, M.; Gilbert, S. E.; Klemenz, C.; Scheel, H. J. *J. Am. Chem. Soc.* **1996**, *118*, 6716.
(31) Li, W.; Liu, C.; Zhou, Y. X.; Bai, Y.; Feng, X.; Yang, Z. H.; Lu, L. H.; Lu, X. H.; Chan, K.-Y. *J. Phys. Chem. C* **2008**, *112*, 20539.
(32) Liu, B.; Boercker, J. E.; Aydil, E. S. *Nanotechnology* **2008**, *19*, 505604.
(33) Liu, B.; Deng, D.; Lee, J. Y.; Aydil, E. S. *J. Mater. Res.* **2010**, *25*, 1588.
(34) Liu, B.; Aydil, E. S. *J. Am. Chem. Soc.* **2009**, *131*, 3985.
(35) Leschkies, K. S.; Divakar, R.; Basu, J.; Enache-Pommer, E.; Boercker, J. E.; Carter, C. B.; Kortshagen, U. R.; Norris, D. J.; Aydil, E. S. *Nano Lett.* **2007**, *7*, 1793.

(36) Yang, H. G.; Zeng, H. C. *J. Am. Chem. Soc.* **2005**, *127*, 270.
(37) Armstrong, R.; Armstrong, G.; Canales, J.; Bruce, P. G. *Angew. Chem., Int. Ed.* **2004**, *43*, 2286.
(38) Wang, X. H.; Li, J.-G.; Kamiyama, H.; Moriyoshi, Y.; Ishigaki, T. *J. Phys. Chem. B* **2006**, *110*, 6804.
(39) Yu, Y.; Yu, J. C.; Chan, C.-Y.; Che, Y.-K.; Zhao, J.-C.; Ding, L.; Ge, W.-K.; Wong, P.-K. *Appl. Catal., B* **2005**, *61*, 1.